NATIONAL ENERGY TECHNOLOGY LABORATORY
OIL & GAS

DOE Award No.: DE-FE0028973

Quarterly Research Performance Progress Report

(Period Ending 3/31/2018)

Advanced Simulation and Experiments of Strongly Coupled Geomechanics and Flow for Gas Hydrate Deposits: Validation and Field Application

Project Period (10/01/2016 to 09/30/2019)

Submitted by:
Jihoon Kim
Jihoon Kim
Signature

The Harold Vance Department of Petroleum Engineering,
College of Engineering
Texas A&M University
501L Richardson Building
3116 College Station TX, 77843-3136
Email: jihoon.kim@tamu.edu
Phone number: (979) 845-2205

Prepared for:
United States Department of Energy
National Energy Technology Laboratory

March 31, 2018

U.S. DEPARTMENT OF ENERGY | NATIONAL ENERGY TECHNOLOGY LABORATORY

Office of Fossil Energy

DISCLAIMER

TABLE OF CONTENTS

ACCOMPLISHMENTS

Objectives of the project

The objectives of the proposed research are (1) to investigate geomechanical responses induced by depressurization experimentally and numerically; (2) to enhance the current numerical simulation technology in order to simulate complex physically coupled processes by depressurization and (3) to perform in-depth numerical analyses of two selected potential production test sites: one based on the deposits observed at the Ulleung basin UBGH2-6 site; and the other based on well-characterized accumulations from the westend Prudhoe Bay. To these ends, the recipient will have the following specific objectives:

1). Information obtained from multi-scale experiments previously conducted at the recipient's research partner (the Korean Institute of Geoscience and Mineral Resources (KIGAM)) that were designed to represent the most promising known Ulleung Basin gas hydrate deposit as drilled at site UBGH2-6 will be evaluated (Task 2). These findings will be further tested by new experimental studies at Lawrence Berkeley National Laboratory (LBNL) and Texas A&M (TAMU) (Task 3) that are designed capture complex coupled physical processes between flow and geomechanics, such as sand production, capillarity, and formation of secondary hydrates. The findings of Tasks 2 and 3 will be used to further improve numerical codes.

2) Develop (in Tasks 4 through 6) an advanced coupled geomechanics and non-isothermal flow simulator ($T+M^{AM}$) to account for large deformation and strong capillarity. This new code will be validated using data from the literature, from previous work by the project team, and with the results of the proposed experimental studies. The developed simulator will be applied to both Ulleung Basin and Prudhoe Bay sites, effectively addressing complex geomechanical and petrophysical changes induced by depressurization (e.g., frost-heave, strong capillarity, cryo-suction, induced fracturing, and dynamic permeability).

Accomplished

The plan of the project timeline and tasks is shown in Table 1, and the activities and achievements during this period are listed as follows along with Table 2.

Task 1: Project management and planning

The fifth quarterly report was submitted to NETL at January 30, 2018. KIGAM has reviewed Subtasks 2.2 and 2.3. LBNL performed an additional experiment for Subtask 3.1. LBNL is working on Subtask 3.2. Also, LBNL has initiated Subtask 3.3. In Subtask 3.5, the experiment is almost finished, and the experimental data are being matched with numerical simulation. We are continuing Subtasks 4.1 and 5.2 related to the experiment of Subtasks 2.1 and 2.4, matching the simulation results with the experimental results. The mid-scale field wide simulation of Ulleung Basin is initiated, and will be compared with the previous studies. The specific status of the

milestones is shown in Table 2. Specific achievements including publication during this period are as follows.

Task 2: Review and evaluation of experimental data of gas hydrate at various scales for gas production of Ulleung Basin

Subtask 2.1 Evaluation of Gas hydrate depressurization experiment of 1-m scale

This task is completed.

Subtask 2.2 Evaluation of Gas hydrate depressurization experiment of 10-m scale

Continuing the previous review of the experiment setup and test, we reviewed the results of the experiment, in particular, effect of the level of depressurization. Fig. 2.2.1 shows the cumulative gas production according to the level of depressurization (DP) ranging from 10 to 40%. There was no consistent tendency of gas production according to the level of depressurization. This behavior indicates that the level of depressurization was insignificant in relation to the gas production behavior. These results are different from the general trends resulting from small-scale experiments which have demonstrated the predominant effect of the level of depressurization on gas production behavior.

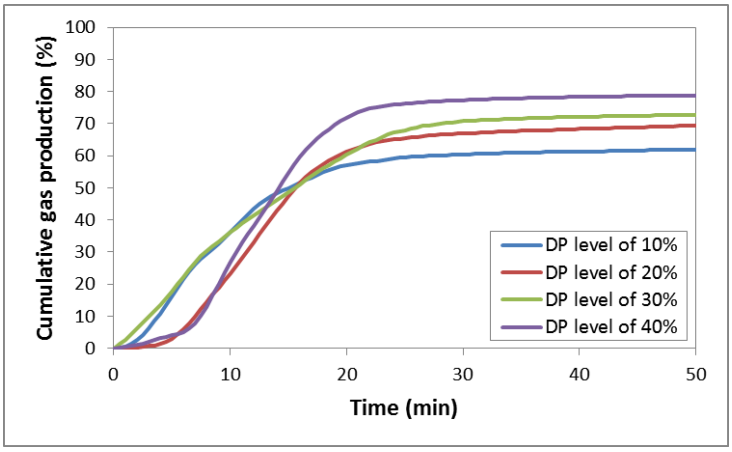

Fig. 2.2.1 Cumulative volume of gas produced according to the level of depressurization (DP) ranging from 10 to 40%

On the other hand, the level of depressurization strongly affected temperature changes during the dissociation process. Fig. 2.2.2 describes the temperature changes with an increasing level of depressurization from 10 to 40%. Temperature drops commonly occurred, as shown in Fig. 2.2.2. The reason for this, as is well known, is that the latent heat of endothermic reaction of

dissociation reduced the temperature, when the sensible heat of the sample was insufficient to decompose the hydrate in the dissociating zone. Subsequently, the reduced temperature commonly returned to the initial value, because heat was continuously transferred from the surroundings; this means that the dissociation lasted thanks to the heat transfer. Remarkably, the higher level of depressurization caused faster changes of temperature reduction and restoration. This was owing to the higher driving force of dissociation for a higher level of depressurization, which accelerated the dissociation process. For this reason, the duration of temperature reduction became shorter while the degree of temperature reduction became larger.

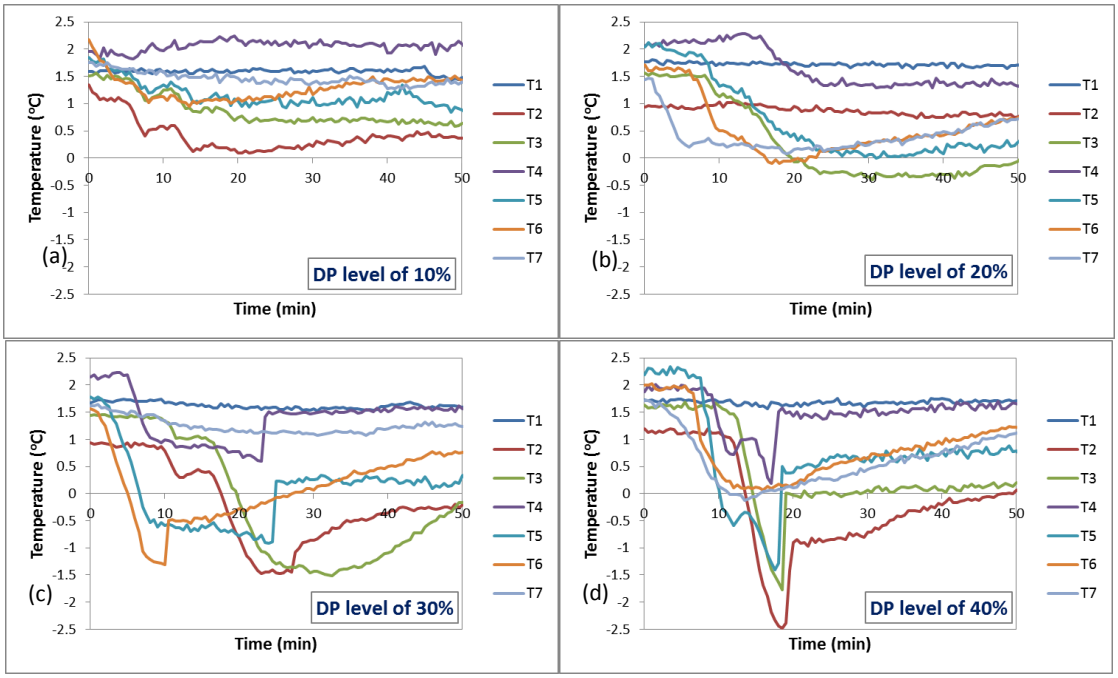

Fig. 2.2.2 Temperature changes with increasing levels of depressurization from 10 to 40%

Subtask 2.3 Evaluation of Gas hydrate depressurization experiment of 1.5-m scale system in 3D

Continuing the previous review of the procedure of this experiment for Subtask 2.3, we have inspected our 3D meter-scale system which includes high pressure cell, data acquisition equipment, fluid control equipment, and temperature control equipment. After confirming that there was no leakage of pressure during the inspection, we packed sediment sample into the 3D meter-scale pressure cell. The packed sediments consisted of alternate layers of clay(30 cm)-

sand(60 cm)-clay(25 cm) representing the layering system in the Ulleung Basin geological structure. We also used artificial particles that mimic the grain size distribution of sandy layers found in the Ulleung Basin, as shown in Fig. 2.3.1

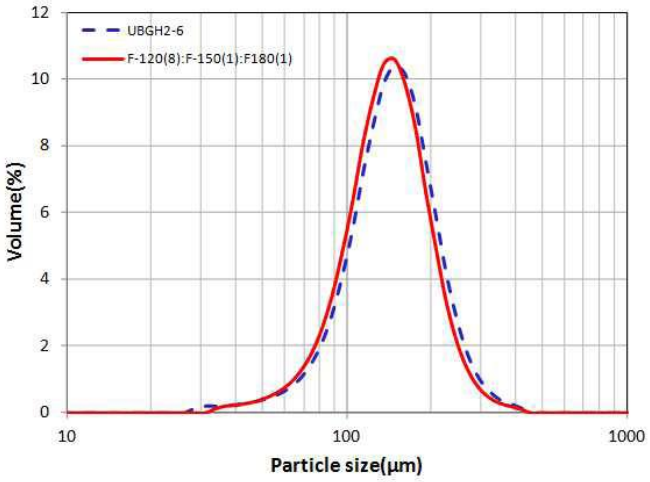

Fig. 2.3.1 Particle size distributions of onsite (Ulleung Basin) and artificial samples

Subtask 2.4 Evaluation of gas hydrate production experiment of the centimeter-scale system

This task is completed.

Task 3: Laboratory Experiments for Numerical Model Verification

Subtask 3.1: Geomechanical changes from effective stress changes during dissociation

We investigated this task further to supplement the previous experiments. Previous experiments examined geomechanical changes in sand and layered samples without hydrate formation. Current experiments extended these to samples where hydrate was formed in sand/mud layered systems. The mud layer was composed of 200g Silt, 50g Kaolinite, 2.5g diatomaceous earth, and 50 mL water. Barium sulfate powder (3 g) was added to the mixture to enhance contrast between the sand and mud layers during CT scanning. The sand layer was F110 sand prepared to 30% water saturation. Particle size analysis of the two samples are listed in Table 3.1.1. Larger particle sizes in the mud layer are likely due to the diatomaceous earth. To make the layered system the

samples were packed into half cylinder forms and frozen (see Fig.3.1.1). The frozen samples were placed in an elastomer sleeve with the mud layer on top and placed into an x-ray transparent pressure vessel (Fig.3.1.2). The confining, inlet and outlet pressures are controlled with syringe pumps, and the temperature and pressure monitored continuously through the experiment (Fig.3.1.3). The entire system was placed on a table in a medical CT scanner and geomechanical changes were monitored by scanning the sample periodically throughout the processes of hydrate formation, saturation, and dissociation. The outlet tube was positioned in the center of the sample, and to prevent sand migration the outlet tube was plugged with an x-ray transparent material.

Results show that in this layered system hydrate primarily forms in the sand layer. To dissociate hydrate, confining pressure was held constant and pore pressure reduced below the hydrate stability point, causing andeffective stress increase from 120 psi to 320 psi. During depressurization dissociation of hydrate occurs with out any appreciable geomechanical changes – the sample density changes were consistent with changes in hydrate/water and size did not shift (see Fig.3.1.4). Effluent samples were taken to observe fines migration, however no particles were observed in the samples and turbidity appeared to be close background. More detailed analysis of the effluent is ongoing.

Table 3.1.1**.** Particle size of mud and sand samples.

Size Classification	Size range	% in mud	% in sand
Clay	Less than 2 um	6.84	0
Silt	2-50 um	59.41	0.03
Very fine sand	50 – 100 um	15.7	18.51
Fine sand	100-250 um	15.9	74.18
Medium sand	250-500 um	2.16	7.28
Coarse sand	500-1000 um	0	0
Very coarse sand	1000-2000 um	0	0

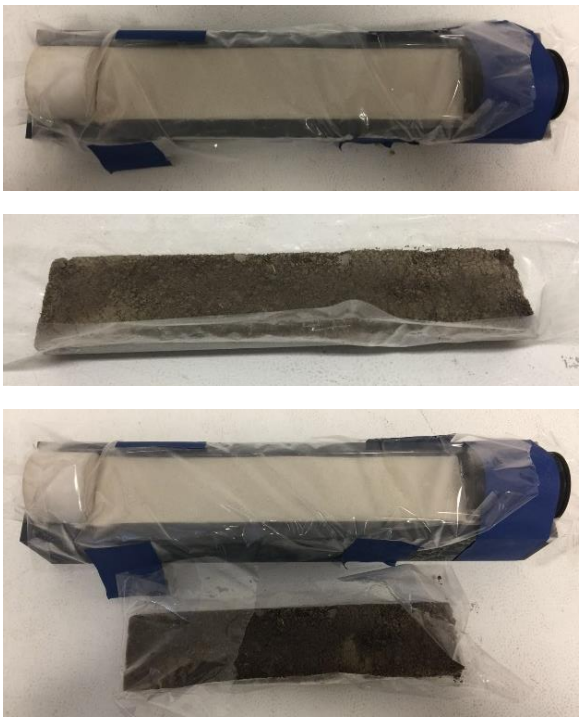

Fig.3.1.1. Layered sample preparation. Top is sand, middle is mud sample, bottom is both. Plastic wrap was used to protect sample and prevent evaporation during freezing.

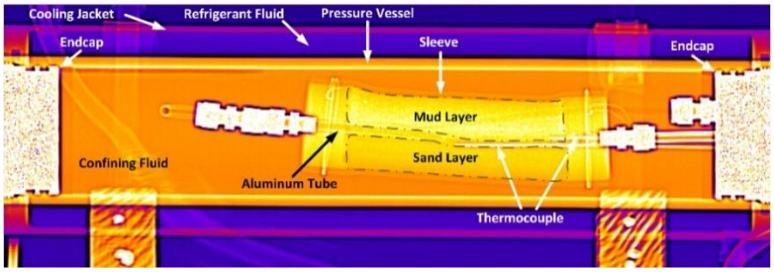

Fig.3.1.2. Details of sample installation in pressure vessel. Sample curvature occurs due to mud compaction.

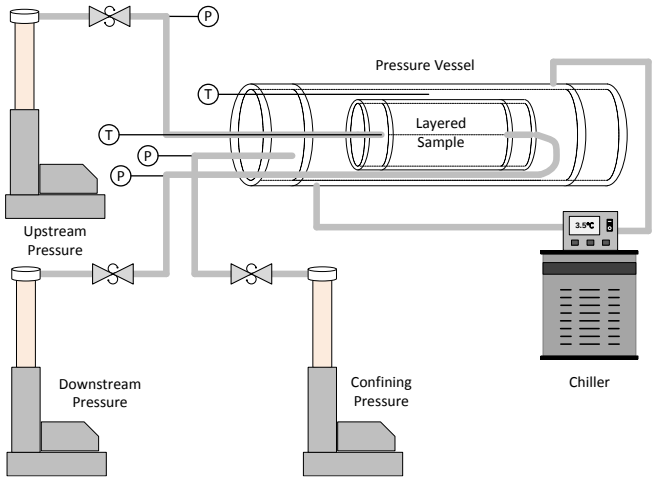

Fig.3.1.3 Schematic of experimental apparatus.

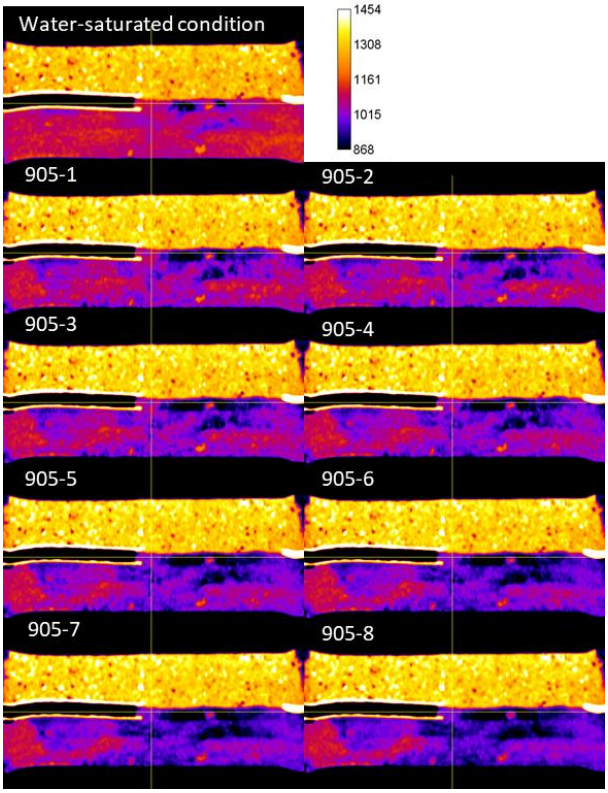

Fig.3.1.4. Sequential CT scan slices (numerical order) of hydrate dissociation in a sand/mud system. The change in density of a layered hydrate system during dissocation is represented by a change in color to darker colors. The sand layer is on the bottom and mud layer is on the top. The scale bar is in Hounsfield units normalized with water = 0.

Subtask 3.2 Geomechanical changes from effective stress changes during dissociation – sand

The same setup and general concept as used in Subtask 3.1 was used, however the plug preventing sand flow was removed and a sand trap was assembled so that flowing sand was not allowed to ruin experimental equipment. In addition, the outlet tube was repositioned to be at the end of the sample. However, removing the plug completely resulted in sample failure before hydrate formation when the effective stress was increased. (see Fig.3.2.1). To stabilize the sample, an Al x-ray transparent screen with mesh size of 0.009 in (0.23 mm) was placed between the sample and the endcap on the outlet end of sample to restrict sand flow but allow for the movement of finer particles. After hydrate formation the sample was saturated with water, followed by water flow (0.5 mL/min) and methane flow (2 mL/min) through the sample and any geomechanical changes were monitored with CT scanning. In addition, a trap was installed downstream from the outlet and water samples from this trap and from the downstream pump were collected and saved for further analysis of turbidity, particle size, and total dissolved solids. This sample showed little or no sand or fines production throughout the experiment, possibly due to the mesh size being too small to allow for migration. A second experiment was performed with a larger mesh screen, this on with a mesh of 0.011 in (0.28 mm). Both screens are larger than the mean particle size of the sand (~110 um). The second experiment showed some density decrease near the outlet (see Fig.3.2.2) indicating some particle movement. Upon disassembly, sand was observed to have moved through the screen and collect on the endcap. Fig.3.2.3 shows the endcap and screen after the experiment.

These results indicate that the sand/mud layered sample is stable during dissociation with only minimal geomechanical changes observed. This may be due to stabilization by the mud layer.

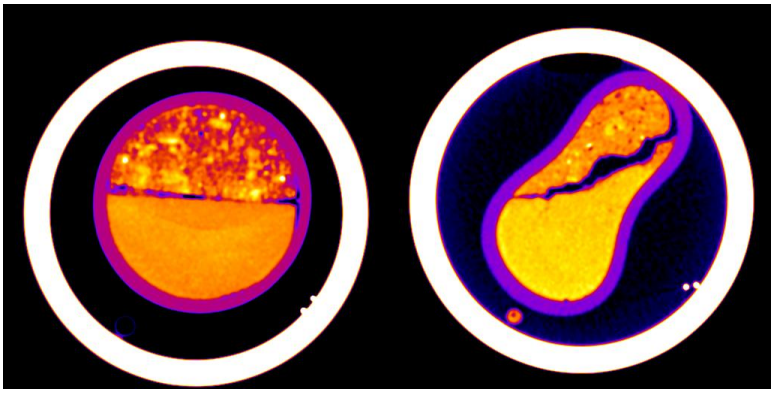

Fig.3.2.1. CT scan cross section mid sample showing failure during setup – no outlet plug installed. Left is before increasing confining pressure, right is when pressure was applied. The sand layer was pushed through the outlet tube into the trap.

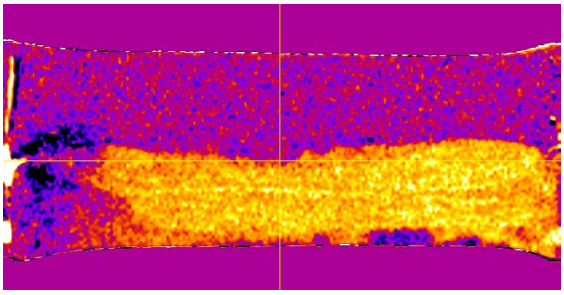

Fig.3.2.2. Layered mud/sand sample after hydrate dissociation. Dark area near the outlet indicates some loss of particles during dissociation.

Fig.3.2.3. Outlet endcap and screen after disassembly showing some sand migration through the screen.

Subtask 3.3 Geomechanical changes resulting from secondary hydrate and capillary pressure changes

Preliminary experiments were performed in support of this task, forming hydrate in a layered system consisting of half mud/half sand with the mud layer oriented on the top as described above. In addition, a custom apparatus has been constructed which will allow the control of temperature in the system. Still to be completed is the core holder which will be designed to provide pressure ports from a number of locations in the core that access the water phase only to monitor the effect of the secondary hydrate formation resulting from the thermal dissociation, and the capillary pressures generated in the process.

Fig.3.3.1 Custom core holder designed to control thermal gradient. The entire sample will be cooled to a consistent temperature to allow hydrate formation. Fluid flowing at a higher or lower temperature flowing through aluminum coil at one end of the sample will allow application of a temperature gradient.

Subtask 3.4 Construction of the Relative Permeability Data in Presence of Hydrate

Not initiated (future year tasks)

Subtask 3.5 Identification of Hysteresis in Hydrate Stability

During this quarter, we have emphasized the simulation and history-matching of the experimental hydrate formation/melting. Thermal properties of the fully-saturated sand pack system in the refrigerator and the associated heat transfer have been fitted. Currently the saturation profiles are being evaluated. As we will show below, we have major progress in determining the total amount of hydrate formation and the hydrate distribution in the sand pack.

Initially the sand pack is saturated by 75% methane gas and 25% stilled water at temperature is 25.3C and at 2,007psia. Gas phase occupies the upper 75% of the sand pack and its saturation is 90%. The water phase occupies the lower 25% of the sand pack and its saturation is considered 100%. At time t=0 the refrigerator temperature is dropped to 1C. The results below shows the experimental data compared to the numerical simulation.

Temperature Pressure and Saturation History in the Sand Pack

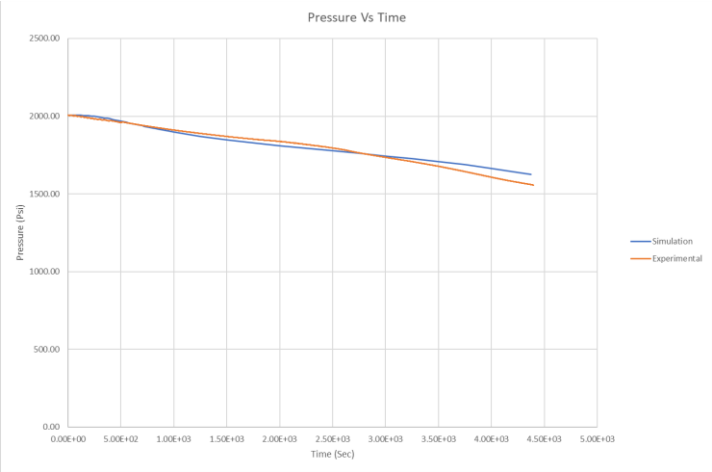

Fig. 3.5.1: Average pressure of the sand pack versus time.

In Fig. 3.5.1 the predicted pressure of the sand pack system is compared to the experimental data. Clearly, pressure drops and this is due to cooling and also due to gas consumption during the hydrate formation. There is less than 10 percent error at 4,400 second, which is at the end of the simulation. This indicates that overall there is good agreement on the sand pack pressure during the total hydrate formation.

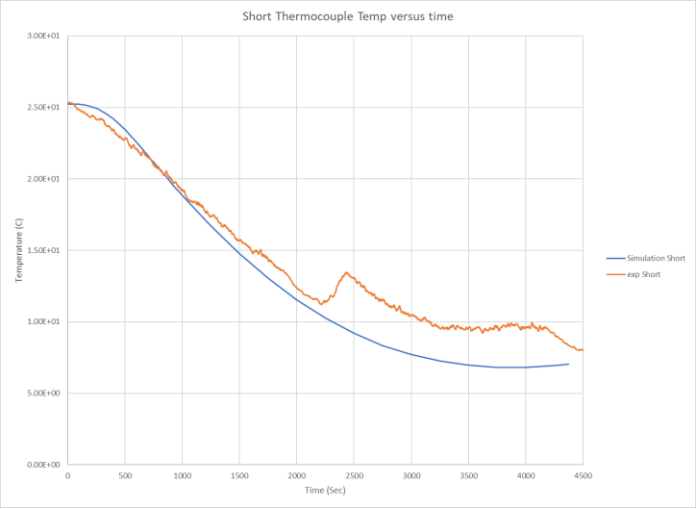

Fig. 3.5.2: Short Thermocouple temperature history

The response of the thermocouple located at the upper portion of the sand pack (i.e., short thermocouple) is shown in Fig. 3.5.2. The short thermocouple fits reasonably well, but it shows a much slower hydrate formation rate than the experimental data. The time of inflection for the

short thermocouple as seen in Fig. 3.5.2 is 3,800 seconds and corresponds to a hydrate saturation in Fig. 3.5.3 of 4 percent.

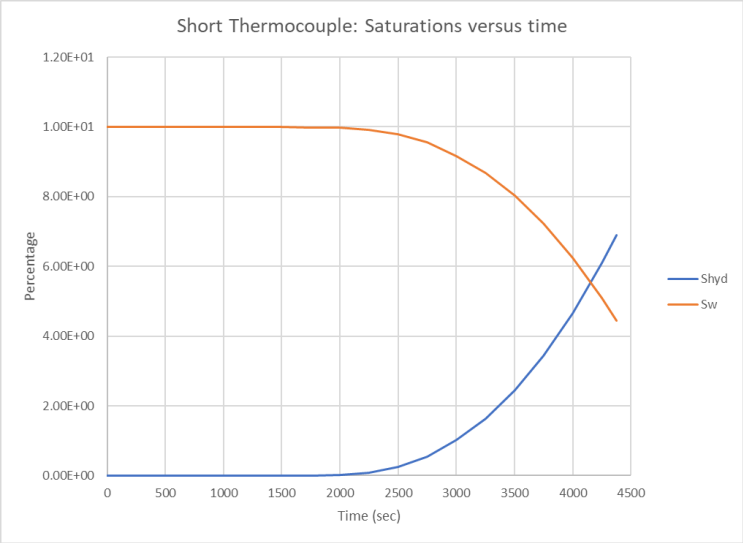

Fig. 3.5.3: Predicted hydrate and water saturation history at the location of the short thermocouple

In Fig. 3.5.3 the hydrate and water saturation profiles for the short thermocouple are shown. There is less hydrate formed at this location, it is not yet clear as to why, sense it started earlier, but there is less formed over all, meaning the rate of formation is less.

Thermocouple Located at the Lower portion of the Sand pack (Long Thermocouple)

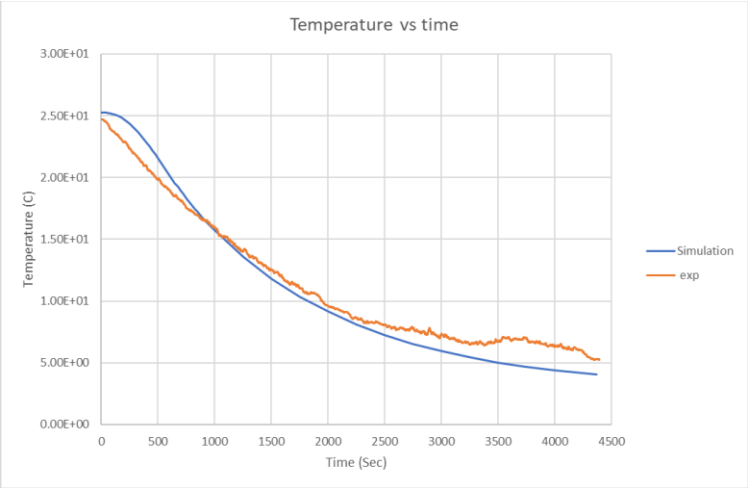

Fig. 3.5.4: Thermal response for Long Thermocouple.

In Fig. 3.5.4 there is good agreement with the measured thermal history up until 2,500 seconds, this region has small amount of gas, and as such it was assumed to have zero gas. Consequently no hydrate forms. However, the experimental data shows small amount of hydrate formation beyond 2,500 seconds. New runs are being made to account for this small hydrate saturation at the lower end of the sand pack.

Pressure versus Temperature Plots for the Sand Pack During Cooling:

Fig. 3.5.5 is more insightful because one can see the temperature variability due to heat transfer and hydrate formation clearly. What was thought of as a small thermal increase in temperature in the temperature history plots turns out to be a quite significant variation on the pressure-temperature plots. Considering the initial cooling period, when the temperature drops from 25C to 10C, the responses of the experimental and numerical systems are close and the difference between their profiles is negligible. This means that the initial heat transfer period, when there is little to no hydrate forming, is in good agreement with the simulation and that the fitting parameters for the heat transfer are known reasonably well. This leaves us with the reaction kinetics parameters and the saturations.

Below 10C we see that the simulator does not predict correctly the experimentally observed temperature peak around 1,600psi. Indeed the kinetics parameters and water-gas ratio needs to be fine-tuned. So far we have observed that the sand pack system is highly sensitive to these quantities.

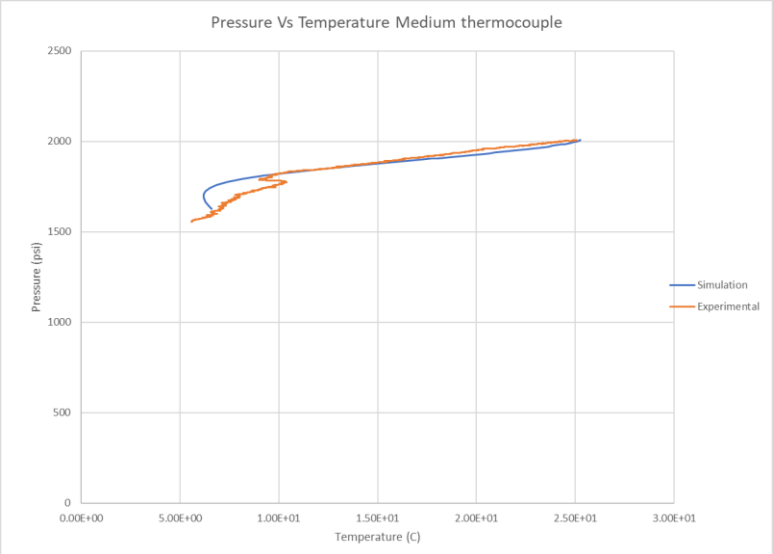

Fig. 3.5.5: Pressure versus Temperature for Medium Thermocouple.

Short Thermocouple

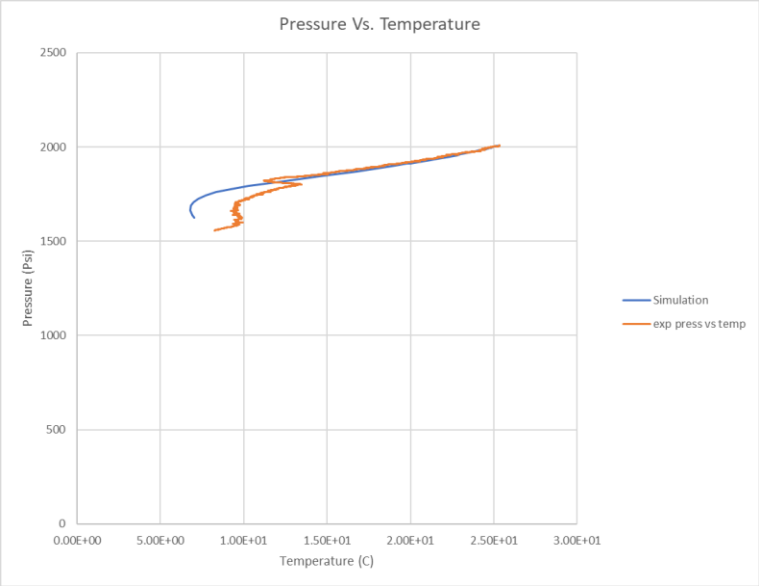

Fig. 3.5.6: Short thermocouple pressure versus temperature.

In the short thermocouple we see in Fig. 3.5.6 roughly the same as in the medium, however the agreement is good only to 12C rather than 10 C. The simulation is giving similar results as the medium thermocouple. We believe this is the case because the gas and water saturation profiles in the medium and upper portion of the sand pack are similar. This is currently being changed to make a more realistic saturation profile but wanted to start simple and get base results.

Long Thermocouple

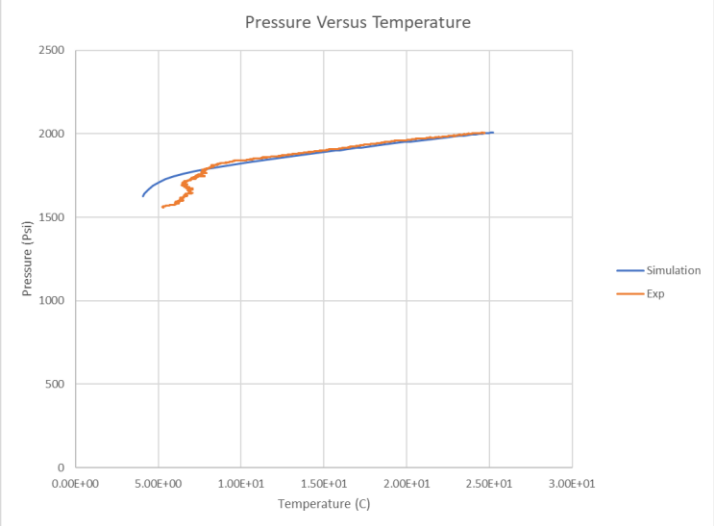

Fig. 3.5.7: Pressure versus temperature for the long thermocouple.

In Fig. 3.5.7, the pressure versus temperature is almost perfect, and the two curves are separated at 8C. This indicates that the assumption of no gas in the lower 25 percent of the sand pack is reasonable but adding a small amount of gas in the lower portion can improve the match.

In conclusion there is good agreement with the thermal response of the sand pack during cooling when there is no hydrate forming. In addition, based on the pressure history-match, there is also a good agreement in the total amount of hydrate formed. The pressure versus temperature results indicate a turning point exists during the cooling, which indicates the heat generation due to hydrate formation. The pressure response indicates that the gas consumption is captured reasonably well in the sand pack and that we should focus to the local heat generation and transfer due to reaction kinetics. This will be done during the next quarter using a history matching and optimization software. At the end of the study, which will be during the early summer, we plan to quantify differences in kinetic parameters due the secondary hydrate formation.

Task 4: Incorporation of Laboratory Data into Numerical Simulation Model

Subtask 4.1 Inputs and Preliminary Scoping Calculations

Continuing the previous work, we have been performing post-processing the data from Subtask 2.1 for numerical simulation. First, we focused on the evolution of displacement for the case of SH=30%, because this case shows relative noticeable displacement while pressure is still constant after the early times. Then, we extracted the corresponding measured data, and are now performing validation with numerical simulation, as shown in Subtask 5.2.

Subtask 4.2 Determination of New Constitutive Relationships

Continuing the previous work, we keep modifying the subroutines of the hysteretic capillarity and relative permeability. Previously, we successfully modeled the stable hysteretic capillary pressure. During this quarter, we have focused on the modeling of the hysteretic relative permeability for cyclic imbibition and drainage for the 1D gas (methane)-water system by using TOUGH+ROCMECH. We calculated dynamic residual saturation from the modeling of capillary pressure. Fig. 4.2.1 shows the evolution of capillary pressure and relative permeability at a monitoring point for the case of the cyclic imbibition-drainage stages with strong capillarity.

We have identified that the updated code provides numerical stability for the proposed hysteresis method, yielding reasonable results. This code will be further tested after we turn on the hydrate option.

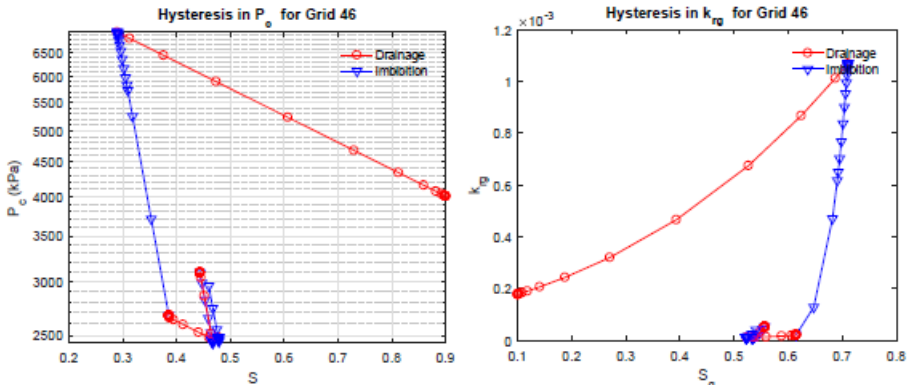

Fig. 4.2.1 Evolution of capillary pressure (left) and relative permeability (right) at a monitoring point.

Subtask 4.3 Development of Geological Model

Not initiated (future research work)

Task 5: Modeling of coupled flow and geomechanics in gas hydrate deposits

Subtask 5.1 Development of a coupled flow and geomechanics simulator for large deformation

This task is completed.

Subtask 5.2 Validation with experimental tests of depressurization

During this quarter, we have been trying to validate T+M, finding matching parameters of geomechanics and flow, conducted in Subtask 2.1. We are using the post-processed data, which was done in Subtask 4.1. Fig. 5.2.1 shows the comparison of vertical displacement between T+M with numerical results from the *uncalibrated* model and experiment data. From the comparison, the simulation result is in the ballpark of the experimental result. Note that we have simplified the experimental condition and scenario, having the constant pressure boundary. We keep matching the numerical results with the experimental data, varying the geomechanical properties.

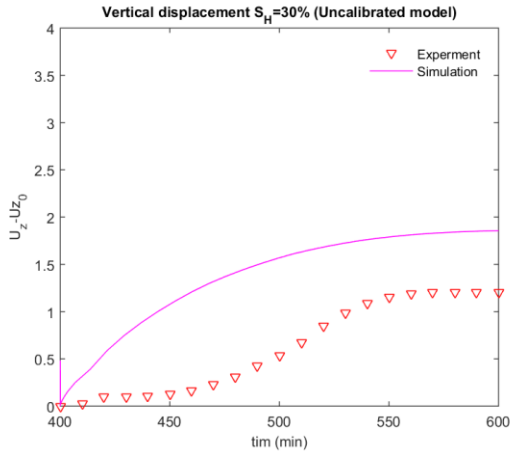

Fig. 5.2.1 Comparison between the experimental data and the results from the uncalibrated model.

Subtask 5.3 Modeling of sand production and plastic behavior

Not initiated (future task).

Subtask 5.4 Modeling of induced changes by formation of secondary hydrates: Frost-heave, strong capillarity, and induced fracturing

In order to simulate the induced fracturing, we have modified the geomechanics simulator, ROCMECH, which can be applied to the unstructured triangular mesh as well. Also, because we employed the sequential method for coupling, we have constructed subroutines for generating the data structure files to communicate between the flow mesh and the geomechanics mesh. We are currently coupling ROCMECH with TOUGH+Hydrate.

Subtasks 5.5 and 5.6 Field-scale simulation of PBU L106 and Ulleung Basin

We have initiated field-wide simulation for the case of Ulleung Basin, first. During this period, we have been constructing the mesh and input files for the 2D axisymmetric coupled flow and geomechanics simulation. Specifically, the 2D axisymmetric domain is discretized with 160 elements in x-direction and 140 in z-direction, respectively, and the total number of gridblocks are 22,400, shown in Fig. 5.5.1. The sea floor is located at z=0m. The multilayered hydrate and mud zones are located between z = -120m and z = -140m, being alternatively deposited.

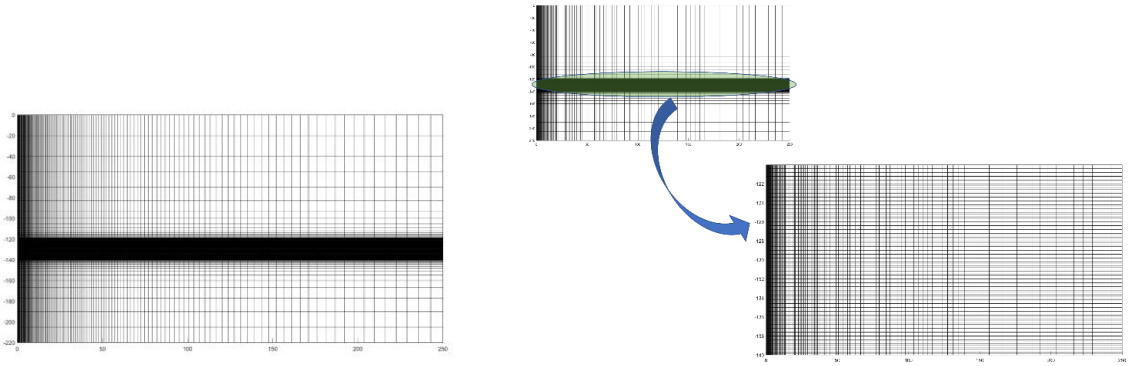

Fig. 5.5.1 The 2D axisymmetric discretized domain. The grid is refined around the vertical well and the hydrate zone.

We have 4 different rock types for the domain: overburden (OVERB), underburden (UNDRB), hydrate (HYD) ,and mud (MUD). The vertical well is located at the very first column of the domain with radius of 0.03 [m]. The constant bottom hole pressure of 15 MPa is applied in the well. The initial pressure of 24.4 MPa is applied at the very first hydrate layer (22nd gridblock in the z direction) and the hydraulic gradient from gravity is applied over the layers. We are currently performing simulation, and will compare the results with the previous studies.

Task 6: Simulation-Based Analysis of System Behavior at the Ignik-Sikumi and Ulleung Hydrate Deposits

Additional analysis of the 2016 production simulations for the UBGH-2-6 field test was recently completed. Using a new method of post-processing analysis, we performed a 1-way coupling of the 2016 production simulation results to the new Millstone geomechanical simulator using the TOUGH-convert analysis package. The results show that:

- The gas release and production rates are generally low and the affected region of the reservoir is limited. The water production accompanying gas production from this deposit appears manageable (in terms of absolute rates and volumes) under all the scenarios investigated in this study; however, in relative terms the water-to-gas ratio is very high during the 14-day production test and stabilizes relatively early.

- The maximum subsidence at the seafloor is predicted to be 0.016m, but the maximum subsidence and uplift of the top and bottom of the reservoir, respectively, is predicted to have a magnitude of 0.22m.

- Reservoir heterogeneity decreases the magnitude of the geomechanical response.

PRODUCTS

Paper published

Kim, J., 2018, A new numerically stable sequential algorithm for coupled finite-strain elastoplastic geomechanics and flow, Computer Methods in Applied Mechanics and Engineering, 335(15): 538-562. This fund is acknowledged.

Paper submitted (under review)

Moridis, G.J., Reagan, M.T., Queiruga, A.F., Kim, S.-J. System Response to Gas Production from a Heterogeneous Hydrate Accumulation at the UBGH2-6 Site in the Ulleung Basin of the Korean East Sea, submitted to Journal of Petroleum Science and Engineering.

Continuing the previous activity of the web-conference, all parties of TAMU, LBNL, KIGAM have been participating in the 2nd International Gas Hydrate Code Comparison Study teleconference (IGHCCS2) held every two weeks online.

BUDGETARY INFORMATION

Table 3 shows the information of the budget for this project and the expenditure up to 03/31/2018.

Table 1 – Initial project timeline and milestones (Gantt Chart)

	FY17				FY18				FY19			
Quarter	Q1	Q2	Q3	Q4	Q1	Q2	Q3	Q4	Q1	Q2	Q3	Q4
Task 1.0. Project Management/Planning	A											
Task 2.0. Experimental study of gas hydrate in various scales for gas production of Ulleung Basin												
Subtask 2.1. Depressurization of 1 m scale in 1D				B								
Subtask 2.2 Depressurization of 10-m scale in 1D							C					
Subtask 2.3. Depressurization of 1.5-m scale in 3D										D		
Subtask 2.4. Revisit to the centimeter-scale system												
Task 3.0. Laboratory Experiments for Numerical Model Verification												
Subtask 3.1. Effective stress changes during dissociation				E								
Subtask 3.2. Sand production								F				
Subtask 33. Secondary hydrate and capillary pressure changes												G
Subtask 3.4. Relative Permeability Data												
Subtask 3.5. Hysteresis in Hydrate Stability												

Task 4.0. Incorporation of Laboratory Data into Numerical Simulation Model												
Subtask 4.1. Inputs and Preliminary Scoping Calculations									H			
Subtask 4.2. Determination of New Constitutive Relationships												
Subtask 4.3. Development of Geological Model												
Task 5.0. Modeling of coupled flow and geomechanics in gas hydrate deposits												
Subtask 5.1 Development of a coupled flow and geomechanics simulator for large deformation				I								
Subtask 5.2 Validation with experimental tests of depressurization										J		
Subtask 5.3 Modeling of sand production and plastic behavior								K				
Subtask 5.4 Frost-heave, strong capillarity, and induced fracturing												L
Subtask 5.5 Field-scale simulation of PBU L106												
Subtask 5.6 Field-wide simulation of Ulleung Basin												
Task 6.0. Simulation-Based Analysis of System Behavior at the Ignik-Sikumi and Ulleung Hydrate Deposits												M

Table 2. Milestones Status

Milestone	Description	Planned Completion	Actual Completion	Status / Comments
Task 1 Milestones				
Milestone A	Complete the kick-off meeting and revise the PMP	12/31/17	1/14/2017	Kickoff meeting held 11/22/17, revised PMP finalized 1/17/17
Task 2 Milestones				
Milestone B	Complete analysis of 1 m-scale experiment in 1D and validation of the cm-scale system (FY17, Q4)	9/30/2017		Completed.
Milestone C	Complete analysis of 10m-scale experiment in 1D	6/30/2018		
Milestone D	Complete analysis of 1.5m-scale experiment in 3D			
Task 3 Milestones				
Milestone E	Complete geomechanical changes from effective stress changes during dissociation and construction of the relative permeability data	9/30/2017		Completed
Milestone F	Complete geomechanical changes from effective stress changes during dissociation (sand production) and hysteresis in hydrate stability	9/30/2018		
Milestone G	Complete geomechanical changes resulting from	9/30/2019		

	secondary hydrate and capillary pressure changes			
Task 4 Milestones				
Milestone H	Complete inputs and preliminary scoping calculations, determination of New Constitutive Relationships, development of Geological Model	12/31/2018		
Task 5 Milestones				
Milestone I	Complete development of a coupled flow and geomechanics simulator for large deformation, validation with experimental tests of Subtasks 2.1 and 2.4.	9/30/17		Completed.
Milestone J	Validation with experimental tests of Task 2 and 3	3/31/2019		
Milestone K	Complete modeling of sand production and plastic behavior, validation with experimental tests of Subtasks 2.2	9/30/2018		
Milestone L	Complete field-scale simulation of the Ulleung Basin and PBU L106	3/31/2019		
Task 6 Milestones				
Milestone M	Complete Task 6	9/30/2019		

Table 3 Budget information

Baselinie Reporting Quarter	Budget Period 1							
	Q1		Q2		Q3		Q4	
	10/01/16-12/31/16		01/01/17-03/31/17		04/01/17-06/30/17		07/01/17-09/30/17	
	Q1	Cumulative Total	Q2	Cumulative Total	Q3	Cumulative Total	Q4	Cumulative Total
Baselinie Cost Plan								
Federal (TAMU)	$37,901	$37,901	$57,809	$95,711	$43,967	$139,678	$34,206	$173,884
Federal (LBNL)	$18,750	$18,750	$18,750	$37,500	$18,750	$56,250	$18,750	$75,000
Non-Federal Cost Share	$6,986	$6,986	$6,986	$13,972	$6,986	$20,958	$656,986	$677,944
Total Planned	$63,637	$63,637	$83,545	$147,183	$69,703	$216,886	$709,942	$926,828
Actual Incurred Cost								
Federal (TAMU)	$0	$0	$10,235	$10,235	$57,085	$67,321	$54,167	$121,488
Federal (LBNL)	$0	$0	$0	$0	$0	$0	$8,500	$8,500
Non-Federal Cost Share	$0	$0	$6,986	$6,986	$6,986	$13,972	$156,986	$170,958
Total incuured cost	$0	$0	$17,221	$17,221	$64,071	$81,293	$219,653	$300,946
Variance								
Federal (TAMU)	($37,901)	($37,901)	($47,574)	($85,475)	$13,118	($72,357)	$19,961	($52,396)
Federal (LBNL)	($18,750)	($18,750)	($18,750)	($37,500)	($18,750)	($56,250)	($10,250)	($66,500)
Non-Federal Cost Share	($6,986)	($6,986)	$0	($6,986)	$0	($6,986)	($500,000)	($506,986)
Total variance	($63,637)	($63,637)	($66,324)	($129,961)	($5,632)	($135,593)	($490,289)	($625,882)

Baselinie Reporting Quarter	Budget Period 2							
	Q1		Q2		Q3		Q4	
	10/01/17-12/31/17		01/01/18-03/31/18		04/01/18-06/30/18		07/01/18-09/30/18	
	Q1	Cumulative Total	Q2	Cumulative Total	Q3	Cumulative Total	Q4	Cumulative Total
Baselinie Cost Plan								
Federal (TAMU)	$42,481	$42,481	$35,307	$77,788	$46,367	$124,155	$39,908	$164,063
Federal (LBNL)	$18,750	$18,750	$18,750	$37,500	$18,750	$56,250	$18,750	$75,000
Non-Federal Cost Share	$6,986	$6,986	$6,986	$13,972	$6,986	$20,958	$6,986	$27,944
Total Planned	$68,217	$68,217	$61,043	$129,260	$72,103	$201,363	$65,644	$267,007
Actual Incurred Cost								
Federal (TAMU)	$35,832	$35,832	$31,662	$67,494				
Federal (LBNL)	$45,952	$45,952	$18,130	$64,082				
Non-Federal Cost Share	$6,986	$6,986	$6,986	$13,972				
Total incuured cost	$88,770	$88,770	$56,778	$145,548				
Variance								
Federal (TAMU)	($6,650)	($6,650)	($3,645)	($10,294)				
Federal (LBNL)	$27,202	$27,202	($620)	$26,582				
Non-Federal Cost Share	$0	$0	$0	$0				
Total variance	$20,552	$20,552	($4,265)	$16,288				

Baselinie Reporting Quarter	Budget Period 3							
	Q1		Q2		Q3		Q4	
	10/01/18-12/31/18		01/01/19-03/31/19		04/01/19-06/30/19		07/01/19-09/30/19	
	Q1	Cumulative Total	Q2	Cumulative Total	Q3	Cumulative Total	Q4	Cumulative Total
Baselinie Cost Plan								
Federal (TAMU)	$43,543	$43,543	$36,189	$79,733	$47,526	$127,259	$41,209	$168,468
Federal (LBNL)	$18,750	$18,750	$18,750	$37,500	$18,750	$56,250	$18,750	$75,000
Non-Federal Cost Share	$6,986	$6,986	$6,986	$13,972	$6,986	$20,958	$6,986	$27,944
Total Planned	$69,279	$69,279	$61,925	$131,205	$73,262	$204,467	$66,945	$271,412
Actual Incurred Cost								
Federal (TAMU)								
Federal (LBNL)								
Non-Federal Cost Share								
Total incuured cost								
Variance								
Federal (TAMU)								
Federal (LBNL)								
Non-Federal Cost Share								
Total variance								

National Energy Technology Laboratory

626 Cochrans Mill Road
P.O. Box 10940
Pittsburgh, PA 15236-0940

3610 Collins Ferry Road
P.O. Box 880
Morgantown, WV 26507-0880

13131 Dairy Ashford Road, Suite 225
Sugar Land, TX 77478

1450 Queen Avenue SW
Albany, OR 97321-2198

Arctic Energy Office
420 L Street, Suite 305
Anchorage, AK 99501

Visit the NETL website at:
www.netl.doe.gov

Customer Service Line:
1-800-553-7681

U.S. DEPARTMENT OF ENERGY | NATIONAL ENERGY TECHNOLOGY LABORATORY